Inlet liner design for a fan noise test rig

André M. N. Spillere*, Danilo S. Braga†, Leonardo A. Seki‡, Lucas A. Bonomo§ and Julio A. Cordioli¶
Federal University of Santa Catarina, Florianópolis - SC, 88040-900, Brazil

Bernardo Martinez R. Junior‖ and Paulo C. Greco Junior**
University of São Paulo, São Carlos - SP, 13566-590, Brazil

Danillo C. dos Reis†† and Eduardo L. C. Coelho‡‡
EMBRAER S.A., São José dos Campos - SP, 12227-901, Brazil

Acoustic liners are a key technology for fan noise control in modern turbofan engines and, even though much research has been done in the last decades, many questions regarding its physics and design process still persist. In order to better understand fan noise sources and their interaction with liners, different test rigs have been developed in the past. The EESC-USP Fan Noise Test Rig has been built at the University of São Paulo to better understand fan noise generation, whereas the UFSC Liner Rig has been developed for impedance eduction of liner samples with grazing flow. In order to gain confidence on the liner design methodology, a liner barrel was designed to achieve optimum fan noise supression at the EESC-USP Fan Noise Test Rig. Based on previous experimental results, the modal content of the Fan Noise Test Rig was considered when defining the optimum impedance, and semi-empirical predictive models of liner impedance were used to design an efficient liner close to the optimum impedance. Flat test samples were then fabricated for measurement with grazing flow at the UFSC Liner Rig. Finally, a liner design was chosen and a liner barrel was fabricated and placed at the EESC-USP Fan Noise Test Rig. Experimental and numerical results show high attenuation levels around the first blade passing frequency.

I. Introduction

Turbofan engines are a major source of noise in aircraft. In special, fan noise is a dominant source at both take-off and approach conditions [1]. Due to its tonal content at the blade passing frequency (BPF) and harmonics, the most common procedure for noise mitigation is the use of acoustic liners at the nacelle internal walls. These materials are composed of a honeycomb layer covered by a perforate face-sheet and backed by a rigid plate, also known as a single degree of freedom (SDOF) liner, and more complex configurations (e.g. two degree of freedom or wire-mesh covered liners) are also largely used. The liner geometry should be selected such that it corresponds to the optimum impedance at certain operating conditions, for instance the fan rotation speed corresponding to full power, flyover or approach conditions [2].

In order to gain confidence in the liner design methodology and very many of the technologies involved, a liner barrel was specified and fabricated for testing at the Fan Noise Rig located at São Carlos School of Engineering, University of São Paulo (EESC-USP). Previous work include a parametric study on the noise levels at the EESC-USP Fan Noise Test Rig [3]. With this in mind, an estimate of the optimum impedance was obtained by means of Cremer's impedance [4], and a semi-empirical impedance models was used to find the corresponding liner geometry [5]. Flat liner test samples were fabricated not only to assess the accuracy of the semi-empirical model, but also to evaluate the liner impedance in the presence of flow. A liner barrel was fabricated based on a selected liner geometry and effective parameters were obtained with the Brüel & Kjaer portable impedance meter. The liner barrel was tested at the EESC-USP Fan Noise

*PhD student, Mechanical Engineering Department, Federal University of Santa Catarina, andre.spillere@lva.ufsc.br.
†PhD student, Mechanical Engineering Department, Federal University of Santa Catarina, danilo.braga@lva.ufsc.br.
‡MSc student, Mechanical Engineering Department, Federal University of Santa Catarina, leonardo.seki@lva.ufsc.br.
§MSc student, Mechanical Engineering Department, Federal University of Santa Catarina, lucas.bonomo@lva.ufsc.br.
¶Professor, Mechanical Engineering Department, Federal University of Santa Catarina, julio.cordioli@ufsc.br.
‖MSc student, Aeronautical Engineering Department, University of São Paulo, bernardo.rocamora@usp.br.
**Professor, Aeronautical Engineering Department, University of São Paulo, pgreco@usp.br.
††Noise and Vibration Engineer, EMBRAER, danillo.reis@embraer.com.br.
‡‡Noise and Vibration Engineer, EMBRAER, eduardo.capucho@embraer.com.br.

Test Rig using an in-duct modal decomposition technique. In this case, modal amplitudes were obtained for hard-walled and lined configurations. Finally, these results were compared to a numerical model using a commercial code.

This work is structured as follows. Section II presents the experimental setup at the University of São Paulo and the Federal University of Santa Catarina. Section III introduces a simple estimate of the optimum impedance for a given operating condition and the corresponding liner design. Section IV shows the fabricated test sample and the results obtained with Brüel & Kjaer portable impedance meter and UFSC Liner Rig. Details of the liner barrel are shown in Section V. Results at the Fan Noise Test Rig are shown in Section VI, and a comparison with a numerical model is presented in Section VI. The main conclusions are outlined in Section VIII.

II. Experimental Setup

A. EESC-USP Fan Noise Test Rig

The EESC-USP Fan Noise Test Rig is a test facility to investigate fan noise sources located at the Department of Aeronautical Engineering of the São Carlos School of Engineering, University of São Paulo. The facility, shown in Figure 1, displays a flexible configuration that allows changes in operational conditions of the rig in order to better isolate noise sources, which allows the analysis each of them individually. The fan stage tested in the EESC-USP Fan Noise Test Rig is a scaled-down replica of the Advanced Control Noise Fan (ANCF) at the Aeroacoustic Propulsion Laboratory facility at NASA Glenn, composed by 16 fan blades and 14 stator vanes. The duct diameter is 0.6 m, except at the fan-stator section, where it contracts to 0.5 m with the purpose of reducing the boundary layer thickness.

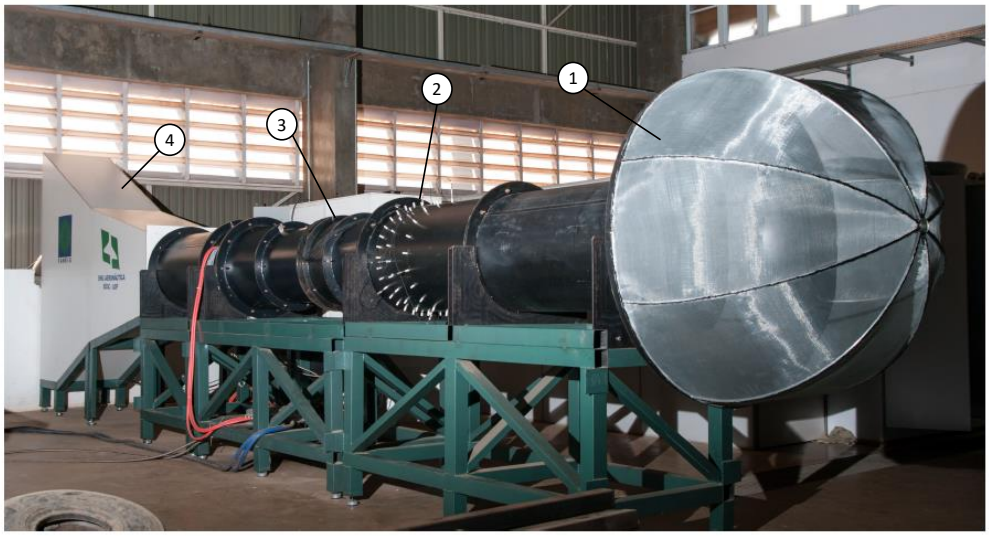

Fig. 1 Photograph of EESC-USP Fan Noise Test Rig setup showing ① inlet, ② microphone array, ③ fan-stator section, ④ exhaust.

Fan speed is set by a software that controls the electric motor inverter constrained to a maximum of 4500 rpm, speed in which the fan is capable of producing axial flows of up to Mach 0.14 in the fan-stator section and tip speeds of around Mach 0.37. Throttling can be set by installing interchangeable screens in the duct exhaust section. A Pitot-static tube Dwyer Series 160E was used for axial flow velocity measurements.

The acoustic measurements were carried out with 1/4" GRAS 40PH and Brüel & Kjaer Type 4958 microphones connected to a National Instruments PXI-1042Q chassis with NI 4496 and NI 4498 module boards. An array of 77 flush-mounted microphones disposed in three circumferential rings is used to capture the sound pressure at the duct walls upstream to the fan. The main objective of the array is to perform sound power measurements and source characterization by means of beamforming techniques [6]. The first ring is composed of 33 equally spaced microphones located 1.43 m upstream to the fan. The second and third rings have 23 and 21 equally spaced microphones, and are located 1.53 m and 1.70 m upstream to the fan, respectively. A schematic view of the test rig is presented in Figure 2.

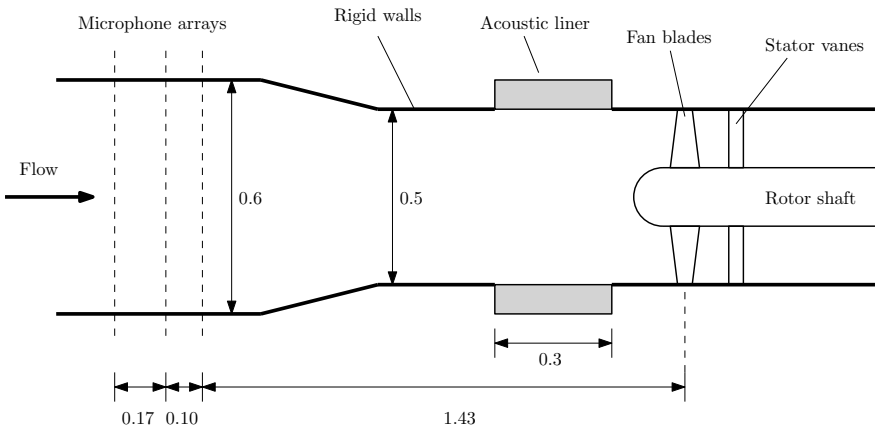

Fig. 2 Schematic view of the EESC-USP Fan Noise Test Rig with a liner barrel. Dimensions in meters.

B. UFSC Liner Rig

The UFSC Liner Rig was developed for impedance eduction of flat liner samples with a length up to 0.21 m. The test rig consists in a duct with rectangular cross section of 0.04 m by 0.10 m divided in modular sections. Figure 3 shows both previous and current versions of the UFSC Liner Rig. The previous version was able to reach flow velocities up to Mach 0.3 and source level up to 140 dB using eight acoustic drivers. The current version, which is used in the work, is able to reach flow velocities up to Mach 0.6 and source level up to 140 dB with a single acoustic driver. Flush-mounted microphones are distributed along the duct in hard-walled and lined sections, so that inverse and direct methods can be used. A schematic view is shown in Figure 4.

(a) Previous test rig.

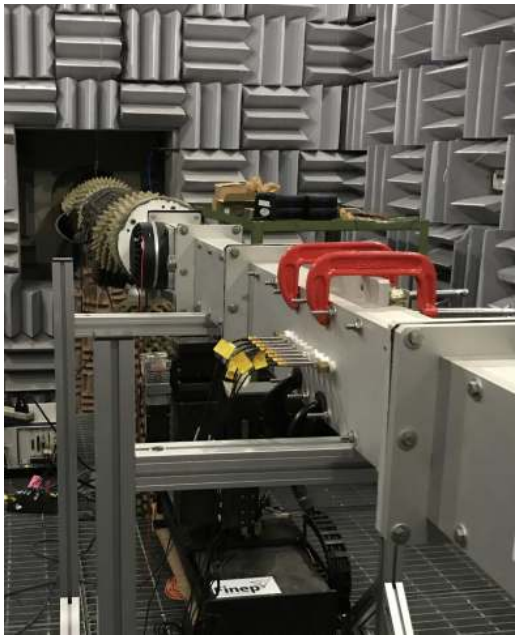

(b) Current test rig.

Fig. 3 Overview of UFSC Liner Rig.

The acoustic field is provided by eight Beyma CP-855Nd compression drivers located upstream and downstream to the liner, and recorded by eight B&K Type 4944-A 1/4" microphones which are also distributed along the test rig. Signal generation and data recording are performed by NI PXI-6723 and PXIe-4499 modules, controlled by an in-house LabView code. Microphones are calibrated with a 94 dB reference source at 1 kHz provided by B&K sound calibrator type 4231. A type T thermocouple placed outside the lined section is used for temperature measurement. Flow is

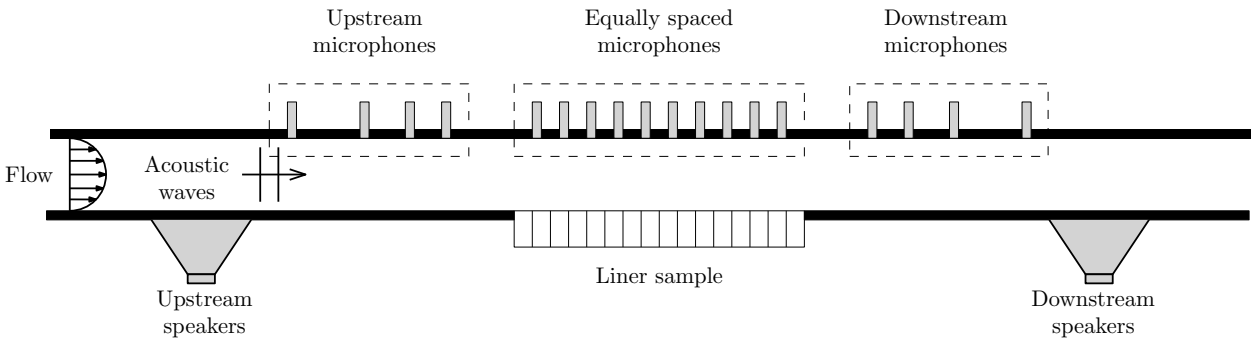

Fig. 4 Schematic view of UFSC Liner Rig.

provided by a pressurized tank and valve opening is controlled by an in-house LabView code to achieve a target Mach number, which has been developed for jet noise investigation. More details of the flow supply system can be found in [7]. A Pitot tube is located at the duct centre-line in the downstream section to monitor flow velocity, which is used in the impedance eduction techniques.

III. Predictive models

It is known beforehand that the EESC-USP Fan Noise Test Rig exhibits, at high rotation speeds, a dominating Tyler-Sofrin mode (2,1) around the first BPF ($f \approx 1000$ Hz) [6]. Also, flow velocity in the test section is found between Mach number of 0.1 and 0.15. In order to find an optimum attenuation, an optimization routine could be considered with aid of numerical simulations or analytic approaches (e.g. mode-matching schemes). In both cases, an accurate description of the noise source modal content would be necessary, since it affects the optimum impedance [2].

Alternatively, a simple estimate is achieved by means of Cremer's impedance [4], which is given by the coalescence of the two least attenuated modes based on infinite lined duct assumption. Tester expanded to high order azimuthal modes [8] and included flow effects in rectangular ducts [9], which are valid in the high frequency limit [10]. In Section III.A, a brief description is given on the optimum impedance in circular ducts with uniform flow considering the exact branch point equation. A full discussion regarding boundary layer effects can be found in [10, 11].

Once the optimum impedance for a desired operating condition is known, the corresponding liner design can be found by means of semi-empirical impedance models. By selecting an appropriate hole diameter and face-sheet thickness, the percentage of open area (POA) and cavity depth are found to match the optimum resistance and reactance. In special, we consider models developed by [5], based on curve-fitting educed impedances at NASA Langley Research Center, and [12], given by curve-fitting in-situ impedances at NLR Aerospace Acoustic Laboratory. A brief description of the models is given in Section III.B. Finally, application of this procedure to EESC-USP Fan Noise Test Rig is shown in Section III.C.

A. Optimum impedance

Consider an infinite lined circular duct with uniform flow in positive direction, cylindrical coordinates (r, θ, x) and locally reacting wall impedance $Z = p/v$. Acoustic propagation in form of $\exp(\mathrm{i}\omega t - \mathrm{i}kx - \mathrm{i}m\theta)$ is governed by the convected Helmholtz equation

$$\frac{\mathrm{d}^2 p}{\mathrm{d}r^2} + \frac{1}{r}\frac{\mathrm{d}p}{\mathrm{d}r} + \left((\omega - Mk)^2 - k^2 - \frac{m^2}{r^2}\right) p = 0, \tag{1}$$

where p is the acoustic pressure, ω is the Helmholtz number, M is the flow Mach number, k is the axial wavenumber and m is the azimuthal wavenumber. The variables have been scaled on duct radius and reference values of density ρ_0 and speed of sound c_0. Solutions to Eq. (1) are given in form of Bessel functions of the first kind J_m. Assuming Ingard-Myers boundary condition [13, 14] at the lined wall leads to the eigenvalue equation

$$\mathrm{i}\omega Z = (\omega - Mk)^2 \, \frac{J_m(\alpha)}{\alpha J_m'(\alpha)}, \tag{2}$$

where $'$ denotes a derivative, and α is the radial wavenumber given by the dispersion relation

$$\alpha^2 = (\omega - Mk)^2 - k^2. \tag{3}$$

Upstream and downstream propagating modes are identified by $\mathrm{Im}(k) < 0$ and $\mathrm{Im}(k) > 0$, respectively. In order to find the location of branch points and the corresponding Cremer's impedance, the derivative of Eq. (2) with respect to α must vanish, which gives the following relation

$$\frac{2MJ_m(\alpha)}{(1-M^2)k + \omega M} + \frac{(\omega - Mk)}{\alpha J'_m(\alpha)} \left[J'_m(\alpha)^2 + \left(1 - \frac{m^2}{\alpha^2}\right) J_m(\alpha)^2 \right] = 0. \tag{4}$$

Eq. (4) has an infinite number of branch points, and therefore care must be taken to select the appropriate value of α. Substituting it in Eq. (2) leads to the optimum impedance, which can be associated to the optimum liner design by means of semi-empirical impedance models.

B. Impedance model

Several semi-empirical impedance models for SDOF liners have been proposed over the years, with special attention to non-linear regimes [15, 16]. A key difference among them is the measurement procedure to obtain experimental data, which can be either in-situ [12, 17] or impedance eduction techniques [5, 18]. Moreover, boundary layer properties have shown to affect the liner impedance [5, 12, 17] and should be carefully taken into account in the impedance model.

1. Kooi and Sarin model

Previous works suggested that skin friction velocity is a better parameter to predict the liner impedance [19]. Therefore, Kooi and Sarin [12] artificially controlled the boundary layer thickness inside the test rig with flow velocities up to Mach 0.45. The semi-empirical model was fitted to experimental results based on the *in-situ* technique [20]. The proposed normalized impedance is given by

$$Z_{\mathrm{KS}} = \frac{\sqrt{8\nu\omega}}{\sigma c_0}\left(\frac{t}{d}\right) + \frac{(5 - t/d)}{4\sigma c_0}(9.9U_* - 3.2fd) + \frac{\mathrm{i}\sqrt{8\nu\omega}}{\sigma c_0}\left(1 + \frac{t}{d}\right) + \frac{\mathrm{i}\omega\,(t+\Delta)}{\sigma c_0} - \mathrm{i}\cot\left(\frac{\omega L}{c_0}\right) \tag{5}$$

where ν is the kinematic viscosity, $\omega = 2\pi f$ is the angular frequency, σ is the POA, c_0 is the speed of sound, t is the face-sheet thickness, d is the hole diameter, L is the cavity depth, and U_* is the skin friction velocity. According to Kooi and Sarin [12], this equation is restricted to a certain range of values. For instance, if $U_*/(ft) < 0.2$ or $u_0/U_* > 4.0$, the resistance term is given by the Guess model [21]. Notice that the ratio between acoustic velocity and skin friction velocity u_0/U_* indicates which term is dominating the non-linear losses [19]. Finally, the hole correction length is given by

$$\Delta = 0.85d(1 - \sqrt{\sigma})\left[0.92 - 0.75\frac{U_*}{ft} + 0.11\left(\frac{U_*}{ft}\right)^2\right]. \tag{6}$$

2. Yu et al. model

In this model,Yu et al. [5] included boundary layer effects by means of the boundary layer displacement thickness δ^*. Moreover, the model has been fitted to experimental data obtained by an impedance eduction method, similar to techniques available at UFSC Liner Rig. The normalized liner impedance is given by

$$Z = \frac{\mathrm{i}\omega(t + \epsilon d)}{\sigma c_0}\left(1 - \frac{4}{k_s d}\frac{J_1(k_s d/2)}{J_0(k_s d/2)}\right)^{-1} + \left(S_1\frac{(1-\sigma^2)}{2(C_D\sigma)^2} - \mathrm{i}S_2\left(\frac{\omega}{\sigma^2}\right)\right)\frac{u}{c_0} + \frac{M}{\sigma\left(2 + 1.256\frac{\delta^*}{d}\right)} - \mathrm{i}\cot\left(\frac{\omega L}{c_0}\right), \tag{7}$$

where $S_1 = 1.336\,541$ and $S_2 = 0.000\,020\,7$ are constants, and M is the mean flow Mach number. The acoustic particle velocity u is found by iteratively solving $u = p/|Z|$. The discharge coefficient C_D can be interpreted as an effective hole area due to the vena contracta formation and is given by

$$C_D = 0.80695\sqrt{\sigma^{0.1}e^{0.5072t/d}}. \tag{8}$$

Also, the Stokes wavenumber k_s is given by

$$k_s = \sqrt{-\frac{\mathrm{i}\omega}{\nu}}, \tag{9}$$

where ν is the kinematic viscosity. Finally, the correction length ϵ is given by

$$\epsilon = \frac{1 - 0.7\sqrt{\sigma}}{1 + 305M^3}. \tag{10}$$

C. Optimum liner

As an example, we consider a liner optimisation for the first BPF corresponding to $f = 1013$ Hz. At this rotation speed, axial flow velocity is found to be $M = 0.1144$. Noise levels in the EESC-USP Fan Noise Test Rig are in the linear regime, so terms related to u in the impedance model are negligible. According to Eq. (4), the optimum impedance for $m = 2$ is $Z = 0.8226 - \mathrm{i}0.4351$. Considering $t = 1.0$ mm, $d = 1.0$ mm and Yu's model, the corresponding liner design has a POA of 3.97 % and a cavity depth of 36.2 mm.

Figure 5 illustrates this process. The optimum resistance increases with frequency, whereas the optimum reactance decreases. By selecting a target frequency, and consequently a target impedance, the corresponding liner design can be found. Note that, in this case, liner resistance almost matches optimum resistance over the whole frequency range. On the other hand, liner reactance matches optimum reactance only once. Flow velocity dependence with rotation speed has been taken into account in both optimum and model impedances. Boundary layer displacement thickness also varies with flow velocity, and has been curve-fitted to measurements at different rotation speeds.

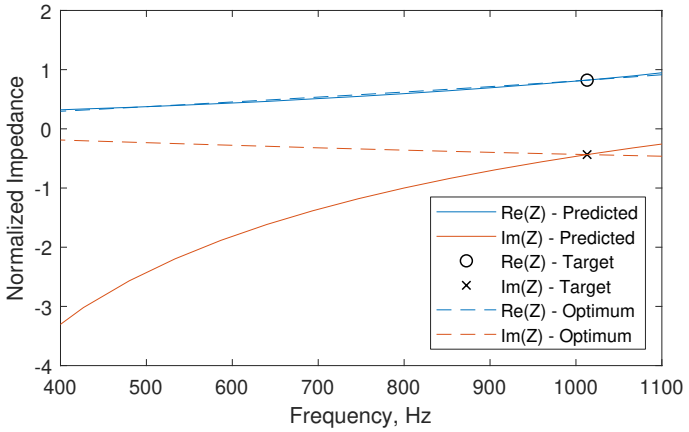

Fig. 5 Optimum impedance variation with BPF. Liner design is selected such that the corresponding impedance curve matches the target impedance.

As a special remark, mode (2,1) is cut-off below frequencies around 650 Hz. Note that, in Figure 5, an optimum impedance has been found in this frequency range. Therefore, care must be taken when using Cremer's impedance concept in the low frequency range.

IV. Liner flat sample

The optimum liner geometry is taken as a reference value to the fabrication of a flat test sample. In reality, such a low porosity is unlikely to be used in a real turbofan engine application. A perforation pattern with nominal $\sigma = 5.67$ % is chosen to be more representative of typical SDOF liners. The effective POA is expected to be lower since the holes are partially blocked by the honeycomb walls. Also, a cavity height of 40 mm is chosen, which increases attenuation at lower frequencies.

In order to asses the accuracy of the impedance model and gain confidence in the fabrication process, five different test samples were designed to cover a wide range of parameters, namely POA and cavity height. The face-sheet thickness and hole diameter were held constant to simplify the manufacturing process. Also, all test samples have a back-plate of 3 mm. In this work, results are shown only for the test sample that corresponds to the liner barrel.

A. Fabrication and assembly

Figure 6 shows the fabrication of a single test sample, including the squared honeycomb and final assembly. In fact, the impact of a squared honeycomb on the liner impedance when compared to a traditional liner is minimal, provided the dimensions remain similar to traditional honeycombs [22]. Each cell has a width of 9.20 mm and wall thickness of 1 mm, which is relatively thick when compared to traditional liners. It is important to note that a great number of holes were partially blocked, thus reducing the effective POA. On the other hand, it is possible to obtain the effective parameters using the BK portable impedance meter, as described in the following section.

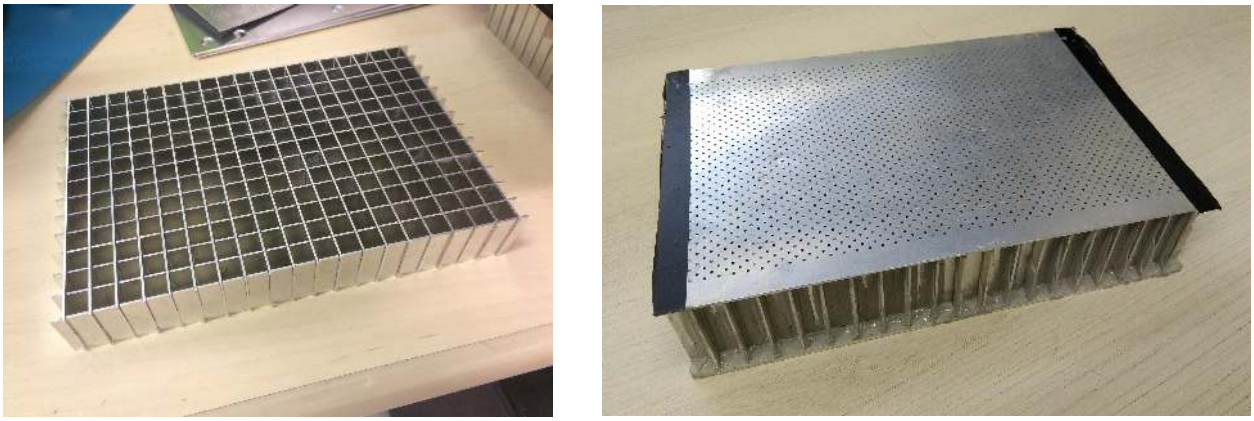

(a) Squared honeycomb. **(b) Final assembly.**

Fig. 6 Liner test sample.

B. Normal incidence impedance measurements

Normal incidence impedance measurements were performed using the BK portable impedance meter, as shown in Figure 7. This system allows quick non-destructive measurements of assembled liner samples in the frequency range between 500 and 6400 Hz and OASPLs up to 155 dB for either pure tone or broadband source [17]. Results include not only impedance spectra for increasing OASPL, but also resistance versus acoustic velocity for a given frequency, which is useful for obtaining the effective POA and the liner non-linearity factor (NLF).

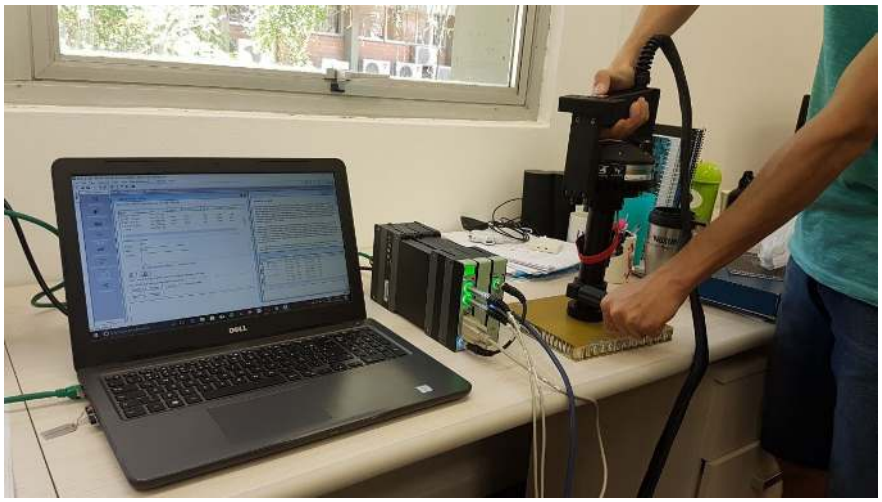

Fig. 7 Liner sample measurement using Brüel & Kjaer portable impedance meter.

1. Effective percentage of open area and non-linearity factor

The face-sheet POA is an essential parameter that controls liner impedance, specially the resistance. Due to the assembly between face-sheet and honeycomb, the holes are partially blocked, leading to an effective POA σ_{eff}. It is possible to estimate it using the Brüel & Kjaer portable impedance meter. By selecting the source to loop with increasing levels of pure tones at an appropriate frequency, it is possible to obtain a resistance curve as a function of acoustic velocity. Therefore, the measured slope a is related to the effective POA by [17]

$$a = \frac{\rho_0}{2(C_D \sigma_{\text{eff}})^2}. \tag{11}$$

In general, $C_D \approx 0.76$ is assumed, although Eq. (8) could also be used. The tone frequency should correspond to the liner resonance frequency [17]. However, due to uncertainties in the low frequency range for this particular liner geometry, tones are generated at higher frequencies higher.

The non-linearity factor (NLF) is defined as the ratio between the resistance at acoustic velocities of 200 cm/s and 20 cm/s. It can be interpreted as a measure of the resistance sensitivity to non-linear effects, namely grazing flow and high SPL. Since the levels in the portable impedance meter are predefined, for instance from 130 to 150 dB with steps of 5 dB, the resistance values at 200 cm/s and 20 cm/s are usually found by curve-fitting to the measured data.

2. Results

Measurements were performed at three different locations to evaluate liner homogeneity. Small differences in local properties are expected, specially for low-porosity liners, in which case the impedance is very sensitive to the impedance meter position. Results compared favorably, and for the sake of brevity only results at the center of the test sample are presented.

Figure 8 shows the impedance spectrum of the test sample with increasing OASPL. It is possible to observe an anti-resonance near 4500 Hz, which corresponds to a cavity height of approximately 38.5 mm, and increasing values of resistance with source level, as expected for non-linear liners. In general, the curves resemble typical impedance spectra of acoustic liners, and hence the fabrication process is considered successful.

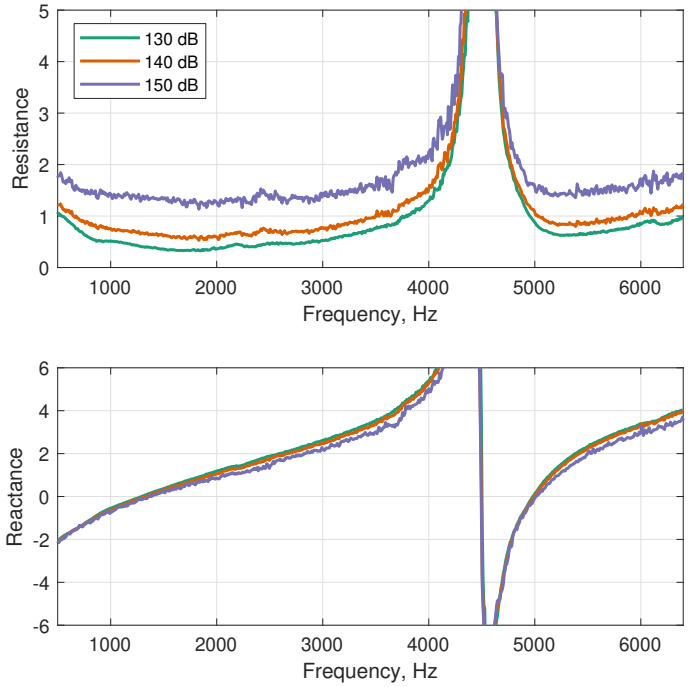

Fig. 8 Impedance spectrum of the flat sample with increasing OASPL.

In order to extract non-linear parameters, measurements were performed with a pure tone at 2000 Hz from 130 dB to 150 dB in steps of 5 dB. Figure 9 shows the acoustic resistance as a function of the acoustic particle velocity at

a frequency of 2500 Hz. The adjusted curve allows to calculate the slope, and therefore the effective POA, which is approximately 4.6 % for $C_D = 0.76$. This result indicates a blockage ratio of approximately 0.8 due to the honeycomb walls. At 150 dB, the acoustic velocity is approximately 85 cm/s, and therefore results were extrapolated to 200 cm/s in order to calculate the NLF. In this case, a value of 4.8 was found, which is in accordance with typical values of SDOF liners.

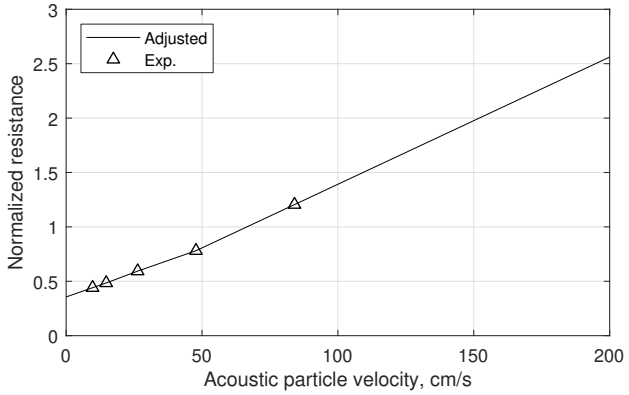

Fig. 9 Resistance of the flat sample as a function of acoustic particle velocity.

C. Grazing incidence impedance measurement

In order to better understand the liner behaviour in the presence of flow, grazing incidence impedance measurements were performed at the UFSC Liner Rig. Both inverse and direct methods were available to educe impedance. The key idea of inverse methods is to find a liner impedance that matches calculated and measured acoustic fields by means of optimisation routines. Over the past years, several procedures have been proposed to calculate the acoustic field, including mode-matching methods [23–25], two-port formulation [26], and frequency domain finite element method [27]. On the other hand, direct methods are based on Prony's method to extract axial wavenumbers in the lined section, thus allowing the straightforward computation of the liner impedance [28–30].

Previous results in the test rig have shown that the direct method with 8 equally spaced microphones performs poorly in the low frequency range, specially below 1000 Hz [31]. Since it corresponds to the liner resonance frequency, the inverse method was chosen to guarantee high accuracy in this frequency range.

1. Impedance eduction

The impedance eduction method used in this work is based on the mode matching technique, inspired by the work of Elnady et al. [24]. A brief description of the method is given as follows.

We consider a bi-dimensional acoustic propagation in a rectangular duct with uniform flow in the positive direction. Transverse and axial coordinates are represented by y and z. Assuming a $\exp(\mathrm{i}\omega t - \mathrm{i}kz)$ dependence, the convected Helmholtz equation is given by

$$\frac{\mathrm{d}^2\hat{p}}{\mathrm{d}y^2} + \left((\omega - Mk)^2 - k^2\right)\hat{p} = 0. \tag{12}$$

The acoustic field at each section $q = 1, 2, 3$ can be written as a sum of downstream (+) and upstream (−) propagating acoustic modes,

$$p^{(q)}(y,z) = \sum_{n=0}^{\infty} A_n^{(q)+}\psi_n^{(q)+}(y)\exp(-\mathrm{i}k_n^{(q)+}z) + \sum_{n=0}^{\infty} A_n^{(q)-}\psi_n^{(q)-}(y)\exp(-\mathrm{i}k_n^{(q)-}z), \tag{13}$$

where A_n are modal amplitudes and $\psi_n^{\pm}(y)$ are the mode shapes, given by

$$\psi_n^{\pm}(y) = \exp(\mathrm{i}\alpha_n y) + \exp(-\mathrm{i}\alpha_n(y-2)), \tag{14}$$

The wavenumbers, normalized by half of the duct height, are found by applying suitable boundary conditions. In case of hard-walled sections, $\alpha_n = n\pi/2$. In the lined section, Ingard-Myers boundary condition [13, 14] leads to

$$\alpha_n \tan(2\alpha_n) = \frac{(\mathrm{i}\omega - \mathrm{i}Mk_n)^2}{\mathrm{i}\omega Z}. \tag{15}$$

Unstable surface waves, as classified by Rienstra [32] and Brambley and Peake [33], are not considered.

Pressure and axial acoustic particle velocity are projected into a test function $\mathcal{W}$ and matched at each interface,

$$\int_{-1}^{1} \mathcal{W}\left(p^{(2)} - p^{(1)}\right) \mathrm{d}y = 0, \quad \int_{-1}^{1} \mathcal{W}\left(p^{(3)} - p^{(2)}\right) \mathrm{d}y = 0, \quad \text{at interface 1-2} \tag{16}$$

$$\int_{-1}^{1} \mathcal{W}\left(u^{(2)} - u^{(1)}\right) \mathrm{d}y = 0, \quad \int_{-1}^{1} \mathcal{W}\left(u^{(3)} - u^{(2)}\right) \mathrm{d}y = 0, \quad \text{at interface 2-3} \tag{17}$$

These matching conditions are not entirely correct, being continuity of mass and momentum at the interface a better description of the physical phenomenon [34]. We assume that such errors remain negligible in the context of impedance eduction techniques. The choice of a suitable test function is important, being the hard-walled acoustic modes a common choice since it forms an orthogonal basis [24]. However, we follow the suggestion from Gabard and Astley [34] by using acoustic modes from the lined section to improve convergence at the interface.

The matching conditions lead to a set of equations to be solved for the modal amplitudes at each interface. Therefore, incident and reflected plane wave amplitudes at the active speaker side and duct termination must be provided, together with an impedance guess. The plane waves amplitudes propagating towards the liner are found by using an over-determined two microphones method. The initial guess is provided by the semi-empirical model described in Section III.B. Once all modal amplitudes are known, acoustic pressure is computed at locations corresponding to microphones in the test rig. From that, a cost function is built,

$$\mathcal{F}(\omega, Z) = \sum_{i=1}^{\mathcal{M}} \left| \frac{p^{(i)}_{\mathrm{meas}}(\omega) - p^{(i)}_{\mathrm{calc}}(\omega, Z)}{p^{(i)}_{\mathrm{meas}}(\omega)} \right|^2, \tag{18}$$

where $\mathcal{M} = 8$ is the number of microphones, p_{meas} and p_{calc} are measured and calculated pressures, respectively. Liner impedance is found when $\mathcal{F}$ is minimized.

2. Results

Liner impedance in the test rig is first compared to results obtained with impedance meter. No flow results are presented in Figure 10 with a downstream acoustic sources. Results with an upstream acoustic source are nearly identical and have been omitted for the sake of brevity. A good agreement is found between test rig and impedance meter over a large frequency range. Small discrepancies can be attributed to local acoustic properties obtained with the impedance meter, whereas results from the test rig indicate a bulk value of the entire test sample. Oscillations in the low frequency range with BK impedance meter are related to sound scattering at the edges of the sample to adjacent honeycomb cells [35]. Predictions with Yu's model [5] using nominal parameters are in better agreement with the test rig results in this frequency range.

Measurements in the presence of grazing flow were performed at averaged flow velocities of $M = 0.19$, which is currently the minimum velocity supported by the flow control system. Although this Mach number is not achieved in the EESC-USP Fan Noise Test Rig, it should indicate the accuracy of impedance semi-empirical models, which are necessary to predict the liner behaviour in the presence of lower flow velocities.

Figure 11 shows results for both upstream and downstream acoustic sources. A small disagreement between educed impedances is found at low frequencies, which has been recently observed by other studies [29–31]. In general, Kooi's model overpredicts the liner resistance. A good agreement is observed between the educed impedance with upstream source and Yu's model. In fact, this model was curve-fitted to educed impedance at NASA Langley Research Center with the same configuration. On the other hand, larger differences are found with a downstream source, which corresponds to the actual problem in EESC-USP Fan Noise Test Rig and turbofan engine inlets. The correct impedance in the presence of flow remains then an open question. However, such discussion is outside the scope of this work.

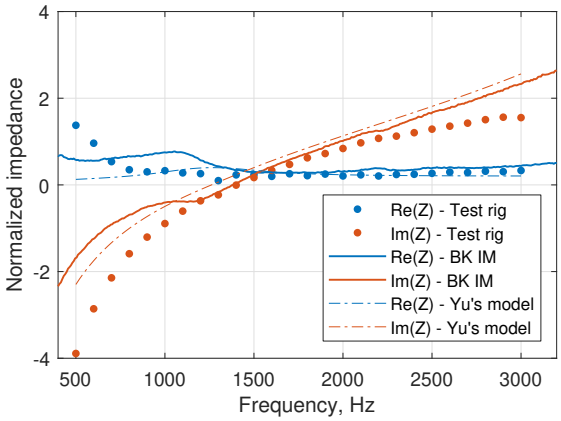

Fig. 10 Comparison between impedance spectra obtained with BK impedance meter, UFSC Liner Rig without flow and prediction from Yu's model [5].

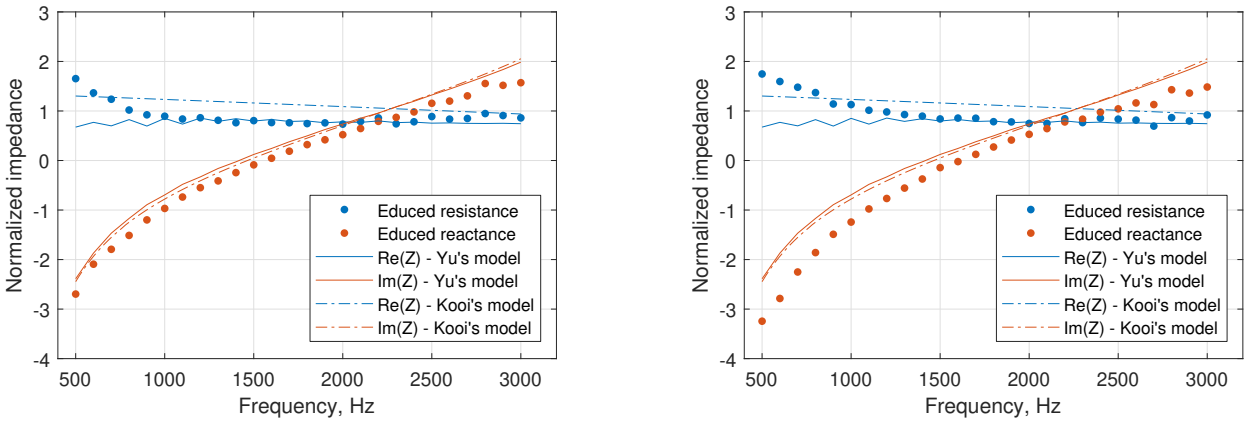

(a) Upstream source. **(b) Downstream source.**

Fig. 11 Comparison between educed impedance and impedance models with flow $M = 0.19$.

V. Liner barrel

Results from the previous section indicate a good agreement between experimental results and predictive models, providing confidence for the liner barrel fabrication. Also, this liner geometry should provide good attenuation around 1000 Hz since the impedance is close to the predicted optimum. The liner barrel was divided into three sections (hereinafter labelled as sections 12, 23 and 13), separated by splices of 1.25 cm width. Photographs of an individual section are shown in Figure 12, including the squared honeycomb and details of the perforated sheet.

A. Quality control

In order to assess the homogeneity of the liner barrel, a quality control was performed at each section using BK impedance meter with a curved flange. Five measurements points were selected and are shown in Figure 13. The acoustic excitation was performed by a broadband noise with 130 dB OASPL between 500 and 6400 Hz which can be considered a linear regime and representative of the liner barrel impedance in the EESC-USP Fan Noise Test Rig.

Based on the measurement of fifteen points, it is possible to obtain the mean value and expanded uncertainty for impedance, NLF, R_{105} and $\mathrm{POA}_{\mathrm{eff}}$. The corresponding t-Student coefficient for 95.45 % confidence is $t = 2.1953$. The final result can be expressed as

$$\mathrm{MR} = \bar{I} \pm tu, \tag{19}$$

where MR is the measurement result, $\bar{I}$ is the mean indication and u is the standard uncertainty. The results for each point and the statistical properties are presented in Table 1. It can be observed that section 12 is nearly uniform, while

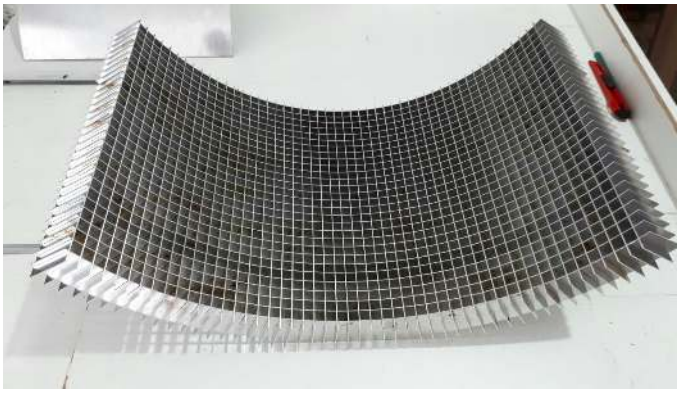

(a) Squared honeycomb assembly.

(b) Perforated face-sheet detail.

Fig. 12 Photographs of the liner barrel.

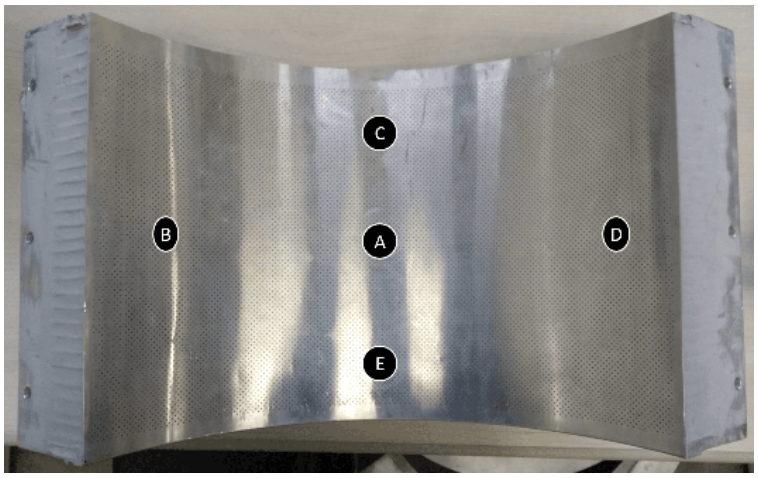

Fig. 13 Measurement points with Brüel & Kjaer portable impedance meter.

13 and 23 present some oscillations. The mean values and corresponding expanded uncertainties are also presented in Table 1.

It is also observed that NLF = 3.67 ± 1.51 is a typical value of perforate liners. Moreover, $\text{POA}_{\text{eff}} = (6.90 \pm 1.75)$ % is similar to the nominal value of 5.67 %. Althouh it may seem counter-intuitive that the effective POA is higher than the nominal value, it must be noted that the selected value of discharge coefficient may not represent this hole geometry. In fact, according to Eq. 8, $C_D \approx 0.86$ for this face-sheet geometry. In this case, the corresponding effective POA is 6.10 %, which is closer to the nominal value. Finally, the cavity height $L = (37.59 \pm 1.91)$ mm is relatively close to the nominal value of 40 mm.

The liner barrel and flat sample impedances are compared in Figure 14. Although most of the flat sample impedance is within the liner barrel confidence interval, some discrepancies are observed. In the high frequency range, it indicates that both liners have different effective geometries. In fact, values of 4.8 for NLF and 38.5 mm for cavity height have been found in the flat sample, which are within the confidence interval, but far from liner barrel mean values. On the other hand, in the low frequency range, which corresponds to the cases investigated at EESC-USP Fan Noise Test Rig, it is difficult to determine the correct liner barrel impedance since uncertainties are high and results between Bk impedance meter and UFSC Liner Rig do not satisfactorily agree.

Table 1 Individual results, mean values and expanded uncertainty.

Section	Point	NLF	POA_{eff} (%)	L (mm)
Section 12	A	4.40	6.54	38.66
	B	3.64	6.23	38.52
	C	3.63	6.64	37.38
	D	3.23	7.60	38.04
	E	3.50	7.38	38.80
Section 13	A	3.68	6.91	38.52
	B	3.19	8.60	37.58
	C	3.65	7.65	36.13
	D	3.19	7.18	37.58
	E	4.84	5.66	37.71
Section 23	A	5.18	5.88	36.25
	B	2.58	7.45	37.19
	C	4.01	6.03	37.38
	D	3.18	6.45	37.84
	E	3.18	7.28	36.25
Mean value, $\bar{I}$		**3.67**	**6.90**	**37.59**
Standard uncertainty, u		**0.69**	**0.80**	**0.87**
Expanded uncertainty, tu		**1.51**	**1.75**	**1.91**

VI. Results at the EESC-USP Fan Noise Test Rig

Although the microphone positions at EESC-USP Fan Noise Test Rig have been chosen for beamforming [6], the experimental analysis can be evaluated by means of a modal decomposition. Such approach is advantageous for several reasons. First, the modal amplitudes in a hard-walled configuration can be estimated and used as an input for analytical and numerical models. Secondly, modal amplitudes in a lined configuration are an indicator of liner performance. Therefore, a good liner design would result in a high attenuation of dominating modes.

The main assumptions of the modal decomposition are listed as follows. The upstream section (inlet) is assumed to be perfectly anechoic. In this case, up to three radial modes for a given azimuthal order can be found, which covers all possible cut-on modes for the first BPF in the whole rotation speed range. This limitation is related to an insufficient number of axial distances between microphones to decompose upstream and downstream propagating modes with $n > 1$. Moreover, modes are assumed to be uncorrelated, which may be inaccurate in the presence of reflections at the duct exit [36].

A. Modal decomposition

As shown in Section III, acoustic propagation in a hard-walled circular duct with uniform flow is governed by the convected Helmholtz equation. In this case, the acoustic field can be expressed as a sum of upstream and downstream propagating modes in form of

$$p(r,\phi,z) = \sum_{m=-\infty}^{\infty}\sum_{n=1}^{\infty}\left(A^{+}_{mn}e^{-\mathrm{i}k^{+}_{mn}z} + A^{-}_{mn}e^{-\mathrm{i}k^{-}_{mn}z}\right)N_{mn}\psi_{mn}e^{-\mathrm{i}m\phi}, \tag{20}$$

where $\pm$ denotes the propagation direction, A_{mn} is the modal amplitude, and N_{mn} is the normalization factor, given by

$$N_{mn} = \frac{\sqrt{2}}{J_m(\alpha_{mn})\sqrt{1-\frac{m^2}{\alpha^2_{mn}}}}, \tag{21}$$

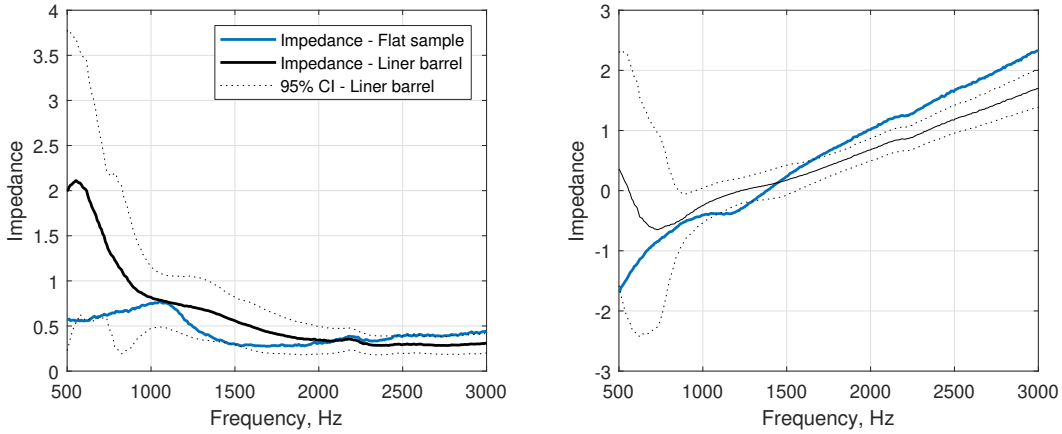

Fig. 14 Impedance comparison between liner barrel and flat sample.

except $N_{01} = \sqrt{2}$. Furthermore, mode shapes must satisfy the hard wall boundary condition $v = 0$, which leads to $J'_m(\alpha_{mn}) = 0$. Once α_{mn} is known, the dispersion relation allows to calculate k_{mn} as follows

$$k^{\pm}_{mn} = \frac{-\omega M \pm \sqrt{\omega^2 - (1 - M^2)\alpha^2_{mn}}}{1 - M^2} \tag{22}$$

Modes that satisfy $\omega^2 \geq (1 - M^2)\alpha^2_{mn}$ are called cut-on modes and carry acoustic energy. The remaining modes are called cut-off modes and decay exponentially. Therefore, only cut-on modes are considered in the modal decomposition.

Pressure at the i-esim microphone is then calculated by

$$p_i = \sum_{j=1}^{N} \left(A^+_j e^{-\mathrm{i}k^+_j z_i} + A^-_j e^{-\mathrm{i}k^-_j z_i} \right) N_j J_{m_j}(\alpha_j r_i) e^{-\mathrm{i}m_j \phi_i}, \tag{23}$$

where N is the number of cut-on modes. Note that modes have been grouped into a single index j, which corresponds to ascending values of α_{mn}. In matrix form, it can be written as

$$\mathbf{p}(\omega) = \mathbf{M}(\omega)\mathbf{A}^{\pm}(\omega), \quad \mathbf{M} = [\mathbf{M}^+ \ \mathbf{M}^-], \tag{24}$$

where $\mathbf{p}$ is the pressure vector at measurement locations, given by the cross-spectral matrix, $\mathbf{A}^{\pm}$ is the modal amplitude vector and $\mathbf{M}$ is the modal matrix of dimension $Q \times 2N$, being Q the number of microphones, given by

$$M^{\pm}_{i,j} = \Psi_{i,j} T^{\pm}_{i,j}, \tag{25}$$

where

$$\Psi_{i,j} = N_j J_{m_j}\left(\alpha_j\right) e^{-\mathrm{i}m_j \phi_i}, \quad T^{\pm}_{i,j} = e^{-\mathrm{i}k^{\pm}_j z_i}. \tag{26}$$

In fact, the condition number of $\mathbf{M}$ indicates the quality of microphone spacing [37]. Neglecting downstream propagating modes and considering only the first BPF, it has been verified that the condition number is approximately 1 at 1400 rpm ($\approx$ 373 Hz) and 5 at 4400 rpm ($\approx$ 1173 Hz) rpm. Finally, the modal amplitudes can be found by

$$\mathbf{A}^- = (\mathbf{M}^-)^{\dagger}\, \mathbf{p}, \tag{27}$$

where † denotes the Moore-Penrose pseudo-inverse.

B. Results

In order to compare both configurations, the lined section was covered with speed tape in order to reproduce a hard-walled configuration. Photographs of both setups are shown in Figure 15. Speed tape was also used at the liner edges and splices to avoid leakage.

Figure 16 presents the modal amplitudes at 4400 rpm. It is clear that, in the hard-walled configuration, a dominant (2,1) mode is present, which corresponds to the Tyler-Sofrin mode, whereas other modes have similar amplitudes. In the lined configuration, this mode is well attenuated, such that lower azimuthal mode orders are the dominating modes. This behaviour is expected since lower order modes have a higher cut-off ratio [38], and are therefore less attenuated [39]. Similar conclusions have been found for other rotation speeds, specially above 3000 rpm, although in these cases liner performance is much less pronounced, as shown in the next section.

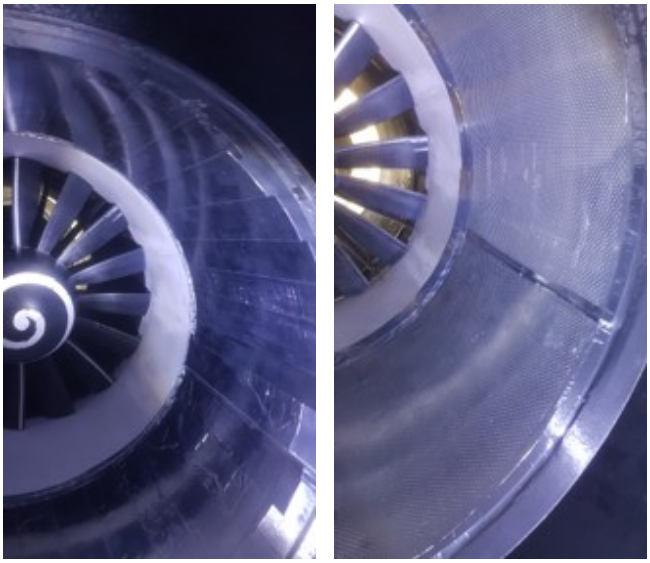

(a) Hard wall **(b) Lined wall**

Fig. 15 EESC-USP Fan Noise Test Rig setup with liner barrel.

VII. Numerical modeling

A numerical finite element model was developed to simulate the conditions in the EESC-USP Fan Noise Test Rig. The model can then be validated using the experimental data collected during the campaign. The procedure adopted is similar to the one described in Acosta et al. [40], which is briefly summarised as follows. The pressure field is governed by the convected Helmholtz equation over a previously computed potential mean flow, with the assumption that the pressure field has no effect on the mean flow. Moreover, Ingard-Myers boundary condition is considered in the lined wall.

A direct frequency analysis was chosen, using the commercial code ACTRAN TM. A three-dimensional mesh with resolution of 18 elements per wavelength at the maximum frequency of interest was created. The analysis only looks at the first BPF, being 4400 rpm the most critical case. The geometry includes the fan plane, lined section with splices, converging section, microphone arrays and an anechoic outlet plane, being the mesh shown in Figure 17. Liner impedance is given by Yu's semi-empirical model considering nominal parameters.

Since the measurements of acoustic pressure in the test rig are taken upstream to the converging section, an inverse procedure using a least squares method fit was adopted to infer the modal content being excited at the rotor plane. Assuming the modal content excited by the rotor to be independent of the hard-walled/lined configuration, this source characterization can be used as an input to the numerical model.

The output of the numerical model is the acoustic pressure at specific points which correspond to the microphone array in the experimental fan rig. The modal decomposition algorithm previously described is then applied to this data to determine the in-duct modal amplitudes. In order to compare liner attenuation at different rotation speeds, the modal acoustic power is introduced [41],

$$\mathcal{P}^{\pm}_{mn} = \pi \left(1 - M^2\right)^2 \frac{\sigma^{\pm}_{mn} |A^{\pm}_{mn}|^2}{\left(1 - M\sigma^{\pm}_{mn}\right)^2}, \tag{28}$$

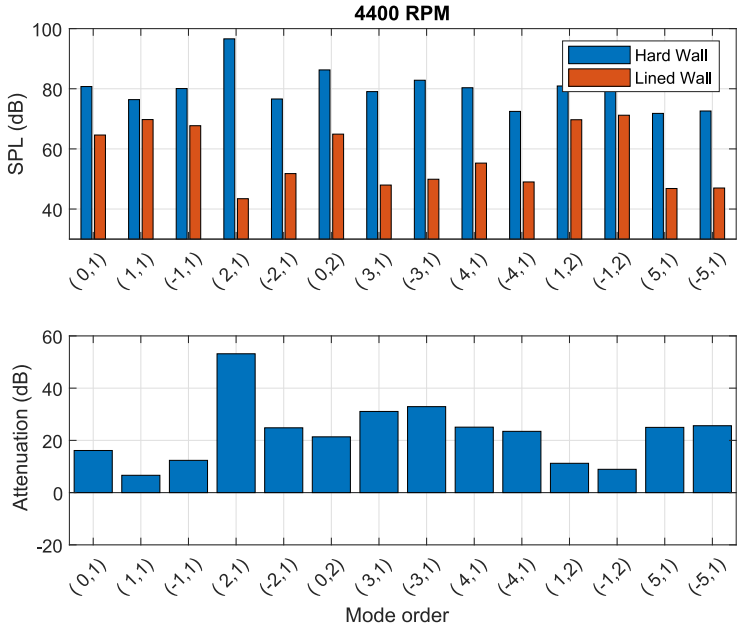

Fig. 16 Modal liner attenuation.

where

$$\sigma_{mn}^{\pm} = \pm\sqrt{1 - \left(1 - M^2\right)\left(\frac{\alpha_{mn}}{\omega}\right)^2} \tag{29}$$

Therefore, liner insertion loss can be evaluated in terms of sound power in dB as the difference between hard-walled and lined configurations,

$$\Delta\text{PWL} = 10\log_{10}\frac{\sum \mathcal{P}^{-}_{\text{hard}}}{\sum \mathcal{P}^{-}_{\text{lined}}}, \tag{30}$$

where only upstream propagating cut-on modes are being considered.

Figure 18 shows the sound power transmission loss for different rotation speeds including experimental results. Although the numerical prediction does not exactly match the measured results, the shape of the curve is reasonably similar. This discrepancy could be explained by an incorrect value of impedance. In fact, results obtained with BK impedance meter have shown that the liner cavity height is smaller, which leads to a higher resonance frequency. Therefore, using effective parameters in the semi-empirical models could lead to a better agreement.

Another possible approach would be to use experimental data from the flat liner sample. However, the flow control system at UFSC Liner Rig is limited to a minimum Mach number of 0.19. Also, it has been shown that educed impedance and semi-empirical model do not agree in the frequency range of interest in the Fan Noise Test Rig. Therefore, a new semi-empirical model would be necessary to correctly predict liner impedance is conditions similar to the Fan Noise Test Rig.

Finally, some neglected effects could also play a role in the current analysis. For instance, it has been shown that boundary layer effects are important when considering upstream propagation [42]. Therefore, including shear flow or more recent boundary conditions [43] could improve the agreement between numerical and experimental results.

VIII. Concluding remarks

In this work, a liner design methodology has been covered using analytical, experimental and numerical tools. A Fan Noise Test Rig, located at the University of São Paulo, was used as a case study to better understand very many of the technologies involved. Steps included i) specification of a desired liner geometry based on the optimum impedance for EESC-USP Fan Noise Test Rig configuration, ii) fabrication and measurements of a flat test sample, iii) fabrication and measurements of a liner barrel, iv) assessment of liner performance at the Fan Noise Test Rig, and v) comparison with a numerical model of the Fan Noise Test Rig. Some concluding remarks are summarised as follows.

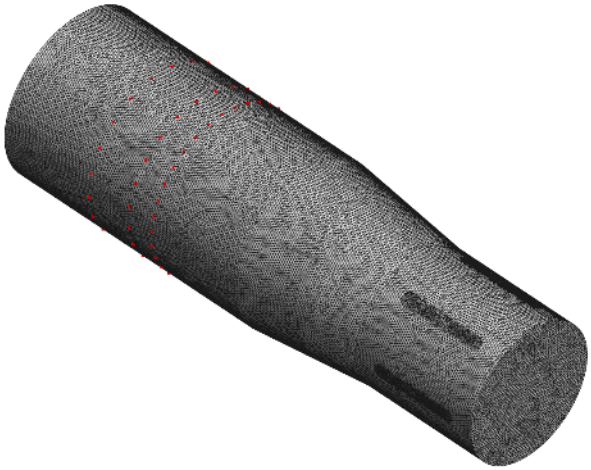

Fig. 17 ACTRAN TM mesh used to solve the finite element model. Red dots correspond to microphone locations.

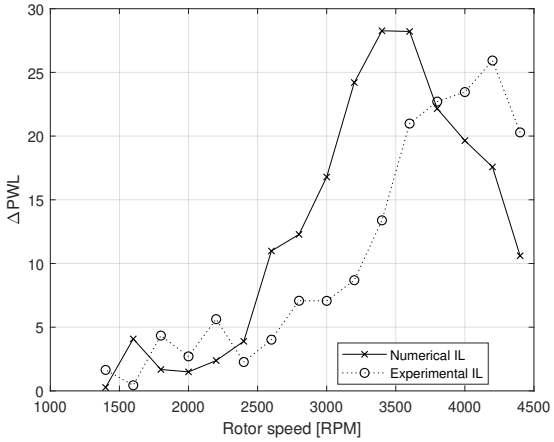

Fig. 18 Comparison of liner insertion loss for numerical and experimental data.

Liner design has been selected based on semi-empirical models to achieve a desired optimum impedance given by the coalescence of the two least attenuated modes in an infinite lined duct. A more accurate optimum impedance could be found by taking into account the actual modal amplitudes at the fan plane and liner length in analytical or numerical models, thus requiring an optimisation routine. However, the high levels of attenuation found in the Fan Noise Test Rig at high rotation speeds suggest that the current approach can provide good results.

Measurements with BK impedance meter have shown that it is possible to extract effective parameters of liner geometry for both flat and curved surfaces, which in turn can be used to improve semi-empirical models and for quality control. On the other hand, impedances obtained with normal incidence may be inaccurate at frequencies up to 1200 Hz due to sound scattering at the edges of the sample, corresponding to the frequency range of interest in the Fan Noise Test Rig.

A comparison between semi-empirical models and educed impedances in the presence of flow indicate that i) the models are not able to predict the increase on resistance at lower frequencies, and ii) the educed impedances using upstream and downstream acoustic sources do not agree in the low frequency range. Therefore, the correct liner impedance at the Fan Noise Test Rig remains an open question. Results obtained with a numerical model of the test rig considering a semi-empirical impedance showed that the frequency of maximum attenuation is incorrectly predicted, such that further investigation is necessary to match experimental and numerical results.

Acknowledgments

The work reported in this article was supported by FINEP (Funding Authority for Studies and Projects), CNPq (National Council for Scientific and Technological Development) and EMBRAER S.A. Authors A. S. and L. B. acknowledge Paul Murray for the instructions on the use of the BK portable impedance meter.

References

[1] Envia, E., "Fan Noise Reduction: An Overview," *International Journal of Aeroacoustics*, Vol. 1, No. 1, 2002, pp. 43–64. doi:10.1260/1475472021502668.

[2] Lafronza, L., McAlpine, A., Keane, A., and Astley, J., "Response Surface Method Optimization of Uniform and Axially Segmented Duct Acoustics Liners," *Journal of Aircraft*, Vol. 43, 2006, pp. 1089–1102. doi:10.2514/1.17727.

[3] Martinez, B., Greco, P. C., Caldas, L., Baccalá, L. A., Cuenca, R. G., and Queiroz, R. L., "Baseline Acoustic Levels of the EESC-USP Fan Rig," *23rd AIAA/CEAS Aeroacoustics Conference*, 2017. doi:10.2514/6.2017-3384.

[4] Cremer, L., "Theorie der Luftschall-Dämpfung im Rechteckkanal mit schluckender Wand und das sich dabei ergebende höchste Dämpfungsma," *Acta Acustica united with Acustica*, Vol. 3, No. 4, 1953, pp. 249–263.

[5] Yu, J., Ruiz, M., and Kwan, H.-W., "Validation of Goodrich Perforate Liner Impedance Model Using NASA Langley Test Data," *14th AIAA/CEAS Aeroacoustics Conference (29th AIAA Aeroacoustics Conference)*, 2008. doi:10.2514/6.2008-2930.

[6] Caldas, L., Greco, P. C., Herold, G., and Baccalá, L. A., "In-duct Rotating Beamforming and Mode Detection of Fan Noise Sources," *22nd AIAA/CEAS Aeroacoustics Conference*, 2016. doi:10.2514/6.2016-3034.

[7] Sirotto, J. R., Cordioli, J. A., and Cavalieri, A. V., "Analysis of far-field coherence of subsonic jet noise," *2018 AIAA/CEAS Aeroacoustics Conference*, 2018. doi:10.2514/6.2018-2977.

[8] Tester, B., "The optimization of modal sound attenuation in ducts, in the absence of mean flow," *Journal of Sound and Vibration*, Vol. 27, No. 4, 1973, pp. 477 – 513. doi:10.1016/S0022-460X(73)80358-X.

[9] Tester, B., "The propagation and attenuation of sound in lined ducts containing uniform or "plug" flow," *Journal of Sound and Vibration*, Vol. 28, No. 2, 1973, pp. 151 – 203. doi:10.1016/S0022-460X(73)80102-6.

[10] Spillere, A. M. N., Zhang, Z., Cordioli, J. A., Åbom, M., and Bodén, H., "Optimum Impedance in the Presence of an Inviscid Sheared Flow," *AIAA Journal*, Vol. 57, No. 3, 2019, pp. 1044–1054. doi:10.2514/1.J057526.

[11] Spillere, A. M., and Cordioli, J. A., "Optimum acoustic impedance in circular ducts with inviscid sheared flow: Application to turbofan engine intake," *Journal of Sound and Vibration*, Vol. 443, 2019, pp. 502 – 519. doi:10.1016/j.jsv.2018.12.007.

[12] Kooi, J., and Sarin, S., "An experimental study of the acoustic impedance of Helmholtz resonator arrays under a turbulent boundary layer," *7th Aeroacoustics Conference*, 1981. doi:10.2514/6.1981-1998.

[13] Ingard, U., "Influence of Fluid Motion Past a Plane Boundary on Sound Reflection, Absorption, and Transmission," *The Journal of the Acoustical Society of America*, Vol. 31, No. 7, 1959, pp. 1035–1036. doi:10.1121/1.1907805.

[14] Myers, M., "On the acoustic boundary condition in the presence of flow," *Journal of Sound and Vibration*, Vol. 71, No. 3, 1980, pp. 429 – 434. doi:10.1016/0022-460X(80)90424-1.

[15] Eversman, W., Nelsen, M. D., Armstrong, D., and Hall Jr., O. J., "Design of Acoustic Linings for Ducts with Flow," *Journal of Aircraft*, Vol. 9, No. 8, 1972, pp. 548–556. doi:10.2514/3.59034.

[16] Motsinger, R., and Kraft, R., "Design and Performance of Duct Acoustic Treatment," *Aeroacoustics of Flight Vehicles: Theory and Practice*, Vol. 2, edited by H. H. Hubbard, NASA Office of Management, Scientific and Technical Information Program, 1991, Chap. 14, pp. 165–206.

[17] Murray, P., and Astley, R. J., "Development of a single degree of freedom perforate impedance model under grazing flow and high SPL," *18th AIAA/CEAS Aeroacoustics Conference (33rd AIAA Aeroacoustics Conference)*, 2012. doi:10.2514/6.2012-2294.

[18] Elnady, T., and Boden, H., "On Semi-Empirical Liner Impedance Modeling with Grazing Flow," *9th AIAA/CEAS Aeroacoustics Conference and Exhibit*, 2003. doi:10.2514/6.2003-3304.

[19] Goldman, A. L., and Panton, R. L., "Measurement of the acoustic impedance of an orifice under a turbulent boundary layer," *The Journal of the Acoustical Society of America*, Vol. 60, No. 6, 1976, pp. 1397–1405. doi:10.1121/1.381233.

[20] Dean, P., "An in situ method of wall acoustic impedance measurement in flow ducts," *Journal of Sound and Vibration*, Vol. 34, No. 1, 1974, pp. 97 – IN6. doi:https://doi.org/10.1016/S0022-460X(74)80357-3.

[21] Guess, A., "Calculation of perforated plate liner parameters from specified acoustic resistance and reactance," *Journal of Sound and Vibration*, Vol. 40, No. 1, 1975, pp. 119 – 137. doi:10.1016/S0022-460X(75)80234-3.

[22] Brown, M. C., and Jones, M. G., "Effects of Cavity Diameter on Acoustic Impedance of Perforate-Over-Honeycomb Liners," *23rd AIAA/CEAS Aeroacoustics Conference*, 2017. doi:10.2514/6.2017-4189.

[23] Aurégan, Y., Leroux, M., and Pagneux, V., "Measurement of Liner Impedance with Flow by an Inverse Method," *10th AIAA/CEAS Aeroacoustics Conference*, 2004. doi:10.2514/6.2004-2838.

[24] Elnady, T., Bodén, H., and Elhadidi, B., "Validation of an Inverse Semi-Analytical Technique to Educe Liner Impedance," *AIAA Journal*, Vol. 47, No. 12, 2009, pp. 2836–2844. doi:10.2514/1.41647.

[25] Buot de l'Épine, Y., Chazot, J.-D., and Ville, J.-M., "Bayesian identification of acoustic impedance in treated ducts," *The Journal of the Acoustical Society of America*, Vol. 138, No. 1, 2015, pp. EL114–EL119. doi:10.1121/1.4923013.

[26] de Santana, L., Roeck, W. D., Desmet, W., and Ferrante, P., "Two-Port Indirect Acoustic Impedance eduction in presence of grazing flows," *17th AIAA/CEAS Aeroacoustics Conference (32nd AIAA Aeroacoustics Conference)*, 2011. doi:10.2514/6.2011-2868.

[27] Watson, W. R., and Jones, M. G., "New Numerical Procedure for Impedance Eduction in Ducts Containing Mean Flow," *AIAA Journal*, Vol. 49, No. 10, 2011, pp. 2109–2122. doi:10.2514/1.J050317.

[28] Jing, X., Peng, S., and Sun, X., "A straightforward method for wall impedance eduction in a flow duct," *The Journal of the Acoustical Society of America*, Vol. 124, No. 1, 2008, pp. 227–234. doi:10.1121/1.2932256.

[29] Renou, Y., and Aurégan, Y., "Failure of the Ingard–Myers boundary condition for a lined duct: An experimental investigation," *The Journal of the Acoustical Society of America*, Vol. 130, No. 1, 2011, pp. 52–60. doi:10.1121/1.3586789.

[30] Weng, C., Schulz, A., Ronneberger, D., Enghardt, L., and Bake, F., "Flow and Viscous Effects on Impedance Eduction," *AIAA Journal*, Vol. 56, No. 3, 2018, pp. 1118–1132. doi:10.2514/1.J055838.

[31] Boden, H., Zhou, L., Cordioli, J. A., Medeiros, A. A., and Spillere, A., "On the effect of flow direction on impedance eduction results," *22nd AIAA/CEAS Aeroacoustics Conference*, 2016. doi:10.2514/6.2016-2727.

[32] Rienstra, S. W., "A classification of duct modes based on surface waves," *Wave Motion*, Vol. 37, No. 2, 2003, pp. 119 – 135. doi:10.1016/S0165-2125(02)00052-5.

[33] Brambley, E. J., and Peake, N., "Classification of aeroacoustically relevant surface modes in cylindrical lined ducts," *Wave Motion*, Vol. 43, No. 4, 2006, pp. 301 – 310. doi:10.1016/j.wavemoti.2006.01.001.

[34] Gabard, G., and Astley, R., "A computational mode-matching approach for sound propagation in three-dimensional ducts with flow," *Journal of Sound and Vibration*, Vol. 315, No. 4, 2008, pp. 1103 – 1124. doi:10.1016/j.jsv.2008.02.015.

[35] Ferrante, P., Roeck, W. D., Desmet, W., and Magnino, N., "Back-to-back comparison of impedance measurement techniques applied to the characterization of aero-engine nacelle acoustic liners," *Applied Acoustics*, Vol. 105, 2016, pp. 129 – 142. doi:https://doi.org/10.1016/j.apacoust.2015.12.004.

[36] Fauqueux, S., and Davy, R., "Modal Deconvolution Method in a Finite Circular Duct, using Flush-mounted Microphones," *2018 AIAA/CEAS Aeroacoustics Conference*, 2018. doi:10.2514/6.2018-3927.

[37] Sack, S., Åbom, M., and Efraimsson, "On Acoustic Multi-Port Characterisation Including Higher Order Modes," *Acta Acustica united with Acustica*, Vol. 102, No. 5, 2016, pp. 834–850. doi:10.3813/AAA.918998.

[38] Tyler, J. M., and Sofrin, T. G., "Axial Flow Compressor Noise Studies," *SAE Technical Paper*, SAE International, 1962. doi:10.4271/620532.

[39] Rice, E. J., "Optimum Wall Impedance for Spinning Modes- A Correlation with Mode Cutoff Ratio," *Journal of Aircraft*, Vol. 16, No. 5, 1979, pp. 336–343. doi:10.2514/3.58528.

[40] Acosta, O., da Silva, A., Cordioli, J. A., and Reis, D., "Numerical investigations of noise radiation from a turbo-fan engine in the presence of hard patches with different geometries," *THE 22nd International Congress on Sound and Vibration. Florence, Italy*, 2015.

[41] Morfey, C., "Acoustic energy in non-uniform flows," *Journal of Sound and Vibration*, Vol. 14, No. 2, 1971, pp. 159–170. doi:10.1016/0022-460X(71)90381-6.

[42] Gabard, G., "Boundary layer effects on liners for aircraft engines," *Journal of Sound and Vibration*, Vol. 381, 2016, pp. 30 – 47. doi:https://doi.org/10.1016/j.jsv.2016.06.032.

[43] Brambley, E. J., "Well-posed boundary condition for acoustic liners in straight ducts with flow," *AIAA Journal*, Vol. 49, No. 6, 2011, pp. 1272–1282. doi:10.2514/1.J050723.